# The effect of distributions of particle nonuniformities on the flow field behind steady normal shock waves

**D. Elata, G. Ben-Dor and O. Igra**
Pearlstone Center for Aeronautical Engineering Studies, Department of Mechanical Engineering, Ben-Gurion University of the Negev, Beer Sheva, Israel

The effect of distributions of nonuniformities in the diameter, heat capacity, and material density of small spherical particles on the properties of a dust-gas suspension passing through a normal stationary shock wave is studied numerically. It was found that the gas temperature is practically independent of the size distribution of the dust particles. The suspension pressure, however, is very sensitive to the size distribution. It rises very sharply when the suspension contains mainly small particles. A distribution in the specific heat capacity of the solid particles results in a minor effect on the velocities and the pressure and in a pronounced effect on the temperature of the solid particles. A distribution in the material density of the solid particles affects both the velocities and the temperatures of the solid and gaseous phases.

**Keywords:** gas-particle suspensions; shock waves

## Introduction

The interest in the gas-dynamic behavior of a gas-particle suspension grew in the past three decades due to its application in many engineering problems. Some typical examples are metalized propellants of rockets, jet-type dust collectors, and blast waves in dusty atmospheres. In addition, mixtures with gases heavily laden with particles occur frequently in industrial processes such as plastics manufacturing, flour milling, coal-dust conveying, powder metallurgy, and powdered-food processing. General descriptions of such flows can be found in Soo,[1] Marble,[2] and Rudinger.[3]

The major differences between the flow fields which are developed behind a normal shock wave in a dusty gas and a pure (dust-free) gas are illustrated in Figures 1a, b for the temperatures and the velocities, respectively. When a steady pure gas encounters a normal shock wave, it experiences a sharp (almost discontinuous) change in its thermodynamic and kinematic properties. This sudden change is shown in Figure 1 to occur between (0) and (1). The thickness of this disturbance, $l_f$, is only a few mean free paths of the gas atoms or molecules. Beyond (1) the gas properties remain constant (solid lines in Figures 1a, b), provided the gas conditions at (1) are not sufficient to excite the internal degrees of freedom of the gas.

If, however, the gas is laden with solid particles, then the suspension which was originally at a state of thermodynamic and kinematic equilibrium, ahead of the shock front, is suddenly changed into a nonequilibrium state because the solid particles, due to their size as compared with $l_f$, do not experience any noticeable change in their properties upon moving from (0) to (1). Thus, at (1) the gas has a much higher temperature than the dust, $T_g \gg T_p$, and a much lower velocity, $u \ll v$ ($u$ is the gas velocity and $v$ is the velocity of the solid particles). Morgenthaler[4] indicated that this is true even if the particle diameter is as small as 0.1 $\mu$m (for shock waves in air at nearly standard conditions, where the mean free path is about 0.066 $\mu$m). Therefore, the particles are not influenced by the initial disturbance, and the gas properties at (1) can be safely assumed to be identical to those of a pure gas with the same initial conditions.

Far downstream of (1), i.e., at ($\infty$) in Figure 1, the gas and the solid phases reach a new state of thermodynamic and kinematic equilibrium via momentum and energy exchange. Theoretically all shock waves in dusty gases are infinitely thick, since equilibrium is approached asymptotically. However, it is a common practice to assign to the shock wave an effective thickness which is defined by a requirement that the suspension properties come close to their equilibrium downstream values. It was shown by Gottlieb and Coskunses[5] that the suspension equilibrium properties (at infinity) can be calculated from the usual normal shock wave relations, provided that the usual pure gas parameters $\gamma$ and $R$ (the specific heat capacities ratio and the specific gas constant) are replaced by effective values $\bar{\gamma}$ and $\bar{R}$ which solely depend on the initial conditions of the suspension. This effective thickness is known in the literature as the relaxation zone, for it is analogous to the relaxation zone in pure gases where the internal degrees of freedom are excited. The extent of the relaxation zone strongly depends on the momentum and heat transfer mechanisms which enable the solid and the gaseous phases to reach a new equilibrium state. The flow behavior in the relaxation zone was studied by many investigators. The pioneering works of Carrier,[6] Kriebel,[7] and Rudinger[8] verified the existence of this relaxation zone and identified the parameters affecting it, namely, the solid particle diameter $D$, its heat capacity $C$, its material density $\sigma$, and the loading ratio $\eta$. Igra and Ben-Dor[9] compared various correlations for the drag coefficient $C_D$ and the heat transfer coefficient Nu, and pointed out their effect on the extent of the relaxation zone. In addition, they studied the role of thermal radiation heat transfer between the two phases and showed that it can be neglected when the incident shock wave Mach number is smaller than 5.

Address reprint requests to Professor Ben-Dor, Pearlstone Center for Aeronautical Engineering Studies, Department of Mechanical Engineering, Ben-Gurion University of the Negev, Beer Sheva, Israel.

Received 19 February 1988; accepted for publication 8 October 1988

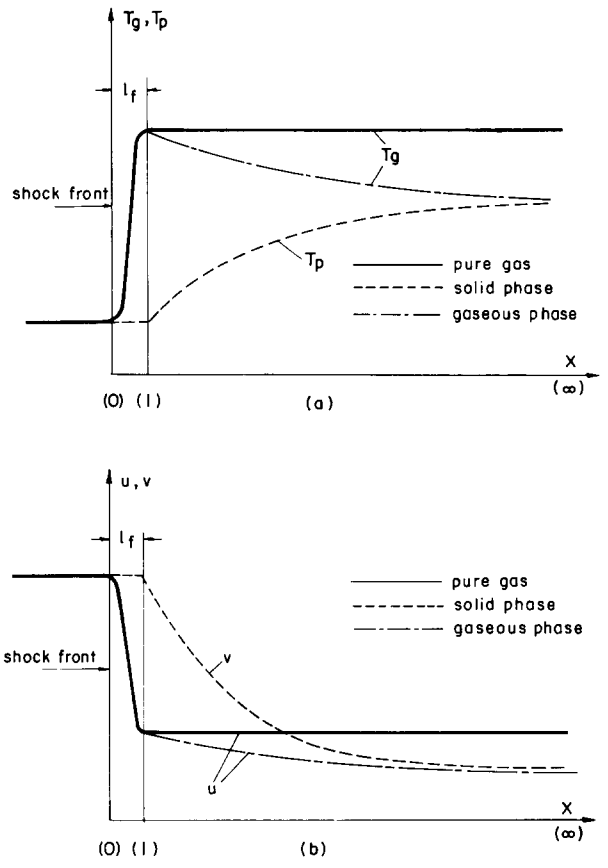


*Figure 1* Shock wave structure in pure and dusty gases

In all the above-mentioned works, as well as in many others, the gaseous phase was assumed to behave as a perfect gas. This assumption was recently relaxed by Ben-Dor and Igra[10] and Igra and Ben-Dor,[11] who solved the flow field while accounting for real gas effects. Dissociating nitrogen was the gaseous phase in the latter work and ionizing argon in the former.

The assumption that the solid particles are inert, which was also adopted in most of the published studies, was also relaxed by Elperin, Ben-Dor and Igra,[12] who solved the flow field of an oxygen-carbon suspension passing through a normal shock wave, behind which the carbon particles reached their ignition temperature and burned out.

In the present study, another commonly used assumption concerning the solid phase is relaxed. It has been a common practice to assume that the solid phase consists of spherical particles of identical diameter $D$, identical material density $\sigma$, and heat capacity $C$. In reality, however, this is not the case, for the particles comprising the solid phase do not have, in general, a uniform size even though they might have the same physical properties (i.e., $\sigma$ and $C$). Furthermore, there could be cases in which the suspension consists of different solid materials (i.e., different values of $\sigma$ and $C$).

The purpose of this study is to numerically investigate the influence of the above-mentioned solid phase nonuniformities on the flow field which is developed behind a normal shock wave.

In the following, the basic assumptions upon which the present model is based are given. The assumptions are followed by the governing equations and the numerical results arising from their solution.

## Theoretical background

### *Assumptions*

The assumptions upon which the present model is based and their implications are as follows:

1. The gaseous phase behaves as an ideal gas. Thus, the equation of state of the gas is $P=\rho_g R T_g$. Note that it is not assumed here that the gas is calorically ideal. Alternatively, the dependence of both $C_p$ and $C_v$ on the gas temperature is accounted for. This has not been done in previous studies, where both $C_p$ and $C_v$ were assumed to be constant.
2. All solid particles are rigid, chemically inert small spheres uniformly distributed in the gaseous phase. Thus there is no heat addition or reduction due to chemical processes between the solid and the gaseous phases. Furthermore, Re and Nu are based on the particle diameter $D$.
3. The volume of the solid phase in the suspension can be neglected. Thus the momentum and energy exchange between the solid particles can be ignored.
4. Aside from momentum and energy interactions between the gaseous and the solid phases, the gaseous phase is considered to be a perfect fluid; i.e., no other viscous or conduction effects are considered.
5. The solid particles are too large to experience any change in their thermodynamic and dynamic properties upon their passage through the shock front. In addition they are also large enough not to experience Brownian motion. Thus, the partial pressure of the solid phase can be neglected.
6. The solid particles are small enough to satisfy the condition $B_i<0.1$, where $B_i$ is the Biot number, $B_i=hr/k_p$ ($h$ is the coefficient of heat transfer, $r$ is the radius of the particle, and $k_p$ is its thermal conductivity). Thus the temperature within the solid particles can be assumed to be uniform.
7. The weight of the solid particles and the buoyancy forces experienced by them are negligibly small in comparison with the drag forces acting on them.
8. The heat capacity $C$ of the solid particles is constant.
9. Ahead of the normal shock wave the suspension is at a state of thermodynamic and kinematic equilibrium; i.e., $u_0=v_0$ and $T_{g0}=T_{p0}$, where $u$ and $v$ are the velocities of the gas and the solid particles, and $T_g$ and $T_p$ are the temperatures of the gas and solid particles, respectively.

In addition, it is assumed that the flow field under consideration is one-dimensional and steady.

### *Governing equations*

The considered suspension is composed of $n+1$ phases. One phase is the gaseous phase. The remaining $n$ phases are all solid phases. Each of the $n$ solid phases consists of identical particles. However, each one of the $n$ solid phases differ from all the other solid phases in at least one of the following properties: the diameter of the solid particle $D$, its material density $\sigma$, or its heat capacity $C$.

Based on the foregoing assumptions the governing equations describing the considered flow field are

Continuity of the gaseous phase

$$\frac{d}{dx}(\rho_g u)=0 \tag{1}$$

Continuity of the $i$th solid phase

$$\frac{d}{dx}(\rho_{pi} v_i)=0 \qquad i=1 \text{ to } n \tag{2}$$

Conservation of momentum of the gaseous phase

$$\frac{d}{dx}(\rho_g u^2 + P) = \sum_1^n F_{Di} \tag{3}$$

Conservation of momentum of the $i$th solid phase

$$\frac{d}{dx}(\rho_{pi} v_i^2) = -F_{Di} \tag{4}$$

Conservation of energy of the gaseous phase

$$\rho_g u \frac{d}{dx}[C_p T_g + \tfrac{1}{2}u^2] = \sum_1^n Q_{pi} + \sum_1^n F_{Di} v_i \tag{5}$$

Conservation of energy of the $i$th solid phase

$$\rho_{pi} v_i \frac{d}{dx}[C_i T_{pi} + \tfrac{1}{2}v_i^2] = -Q_{pi} - F_{Di} v_i \tag{6}$$

Equation of state of the gaseous phase

$$P = \rho_g R T_g \tag{7}$$

In the above equations $\rho_g$, $u$, $T_g$, and $P$ are the density, velocity, temperature, and pressure of the gaseous phase, respectively, $\rho_{pi}$, $v_i$, and $T_{pi}$ are the spatial density, velocity, and temperature of the $i$th solid phase, respectively. Note that the material density of the solid particles is $\sigma_i$, which can be related to the spatial density $\rho_{pi}$ via the relation $\rho_{pi} = n_i V_{pi} \sigma_i$ where $n_i$ is the number density of the $i$th solid particle and $V_{pi}$ is the volume of a single $i$th solid particle. According to assumption 5, the partial pressures of all the solid phases are zero. For this reason $P$ is not only the pressure of the gaseous phase, but the pressure of the suspension as well. $C_p$ and $R$ are the specific heat capacity at constant pressure and the specific gas constant of the gaseous phase, and $C_i$ is the heat capacity of the particles of the $i$th solid phase. $F_{Di}$ is the drag force per unit volume exerted by the gaseous phase on the particles of the $i$th solid phase, and $Q_{pi}$ is the heat transferred per unit volume from the particles of the $i$th solid phase to the gaseous phase.

The drag force $F_{Di}$ can be calculated from

$$F_{Di} = \tfrac{3}{4}\rho_g \rho_{pi}(v_i - u)|v_i - u| C_{Di}/D_i \sigma_i \tag{8}$$

where $D_i$ is the diameter of the solid particle, $\sigma_i$ is their material density, and $C_{D_i}$, the drag coefficient,

$$C_{D_i} = 0.48 + 28\,\mathrm{Re}_i^{-0.85} \tag{9}$$

The slip Re number for the $i$th solid phase is

$$\mathrm{Re}_i = \frac{\rho_g |v_i - u| D_i}{\mu_g} \tag{10}$$

where the dynamic viscosity $\mu_g$ depends on the gas temperature $T_g$.

The transferred heat $Q_{pi}$ can be calculated from

$$Q_{pi} = 6 h_i \rho_{pi}(T_{pi} - T_g)/D_i \sigma_i \tag{11}$$

where $h_i$, the coefficient of convection heat transfer, can be obtained from

$$h_i = \frac{k_g \mathrm{Nu}_i}{D_i} \tag{12}$$

$\mathrm{Nu}_i$ is the Nusselt number of the $i$th solid phase:

$$\mathrm{Nu}_i = 2 + 0.459\,\mathrm{Pr}^{0.33}\,\mathrm{Re}_i^{0.55} \tag{13}$$

where Pr is the Prandtl number

$$\mathrm{Pr} = \frac{\mu_g C_p}{k_g} \tag{14}$$

and $k_g$ is the thermal conductivity of the gaseous phase.

The above set of governing equations consists of $4+3n$ equations (conservation of mass, momentum, and energy for the gaseous phase, equation of state of the gaseous phase and conservation of mass, momentum, and energy for each of the $n$ solid phases). The number of the unknowns is also $4+3n$ ($\rho_g$, $u$, $T_g$, and $P$ for the gaseous phase and $\rho_{pi}$, $v_i$, and $T_{pi}$ for each of the $n$ solid phases). Thus the set of governing equations is solvable in principle.

## Numerical approach

### *Computer code*

There are many computational packages capable of numerically solving differential equations. The one chosen for solving the differential equations governing the problem at hand is the IMSL (International Mathematical & Statistical Libraries) package, which can run on a CDC Cyber 840 computer. The IMSL package contains three computer codes for solving differential equations with given initial conditions:

DVERK—based on the Runge-Kutta method, and recommended for cases where high accuracy is not required and where the derivatives can be simply calculated.

DGEAR—based on the predictor-corrector method. Although it results in poor accuracy, it is preferable to DVERK when the calculation of the derivatives is difficult and hence expensive.

DREBS— based on the extrapolation method. Preferable when high accuracies are required and when the derivatives can be calculated in a relatively simple and inexpensive way.

The DREBS code was adopted in the present study. This code performs a triple check of the obtained error between each two extrapolation steps. Since the DREBS code is limited to the case where each derivative is independent of the other derivatives, the governing equations need to be rearranged. The rearrangement of the governing Equations 1 to 7 results in

$$\frac{dT_g}{dx} = \frac{\sum_1^n \left(Q_{pi} + F_{Di} v_i - \dfrac{F_{Di} u^3}{u^2 - RT_g}\right)}{\rho_g u \left(C_p - \dfrac{Ru^2}{u^2 - RT_g}\right)} \tag{15}$$

$$\frac{du}{dx} = \frac{\sum_1^n F_{Di} - \rho_g R \dfrac{dT_g}{dx}}{\rho_g \dfrac{u - RT_g}{u}} \tag{16}$$

$$\frac{dP}{dx} = \rho_g R\left(\frac{dT_g}{dx} - \frac{T_g}{u}\frac{du}{dx}\right) \tag{17}$$

$$\frac{d\rho_g}{dx} = \frac{\rho_g}{u}\frac{du}{dx} \tag{18}$$

$$\frac{dT_{pi}}{dx} = \frac{Q_{pi}}{C_i \rho_{pi} v_i} \tag{19}$$

$$\frac{dv_i}{dx} = \frac{F_{Di}}{\rho_{pi} v_i} \tag{20}$$

$$\frac{d\rho_{pi}}{dx} = \frac{\rho_{pi}}{v_i}\frac{dv_i}{dx} \tag{21}$$

Note that although Equations 15 to 21 do not reflect the dependence of the gas specific heat capacity on its temperature since a space gradient of $C_p$ does not appear, the value of $C_p$

was calculated at any position $x$ according to the temperature at that position. This procedure assumes that the space gradient of $C_p$ is neglectable.

## Initial conditions

As mentioned earlier the properties of the solid phases do not change when they pass through the normal shock wave. Thus, the solid particles velocity $v_i$, temperature $T_{pi}$, and spatial density $\rho_{pi}$ immediately behind the shock front remain identical to their appropriate values ahead of the shock front; i.e.,

$$(v_i)_1=(v_i)_0 \quad (T_{pi})_1=(T_{pi})_0 \quad (\rho_{pi})_1=(\rho_{pi})_0 \tag{22}$$

Furthermore, the multiphase suspension is assumed to be in thermodynamic and kinematic equilibrium ahead of the shock front; therefore $(v_i)_0=u_0$, $(T_{pi})_0=T_0$, and $(\rho_{pi})_0=\eta_i\rho_{g0}$, where $\eta_i$ is the loading ratio of the $i$th solid phase.

The properties of the gas, on the other hand, change almost discontinuously across the shock wave. The gas properties immediately behind the shock front can simply be calculated from the normal shock jump conditions; i.e.,

$$\frac{P_1}{P_0}=\frac{2\gamma M_0^2}{\gamma+1}-\frac{\gamma-1}{\gamma+1} \tag{23}$$

$$\frac{\rho_{g1}}{\rho_{g0}}=\frac{(\gamma+1)M_0^2}{(\gamma-1)M_0^2+2} \tag{24}$$

$$\frac{T_{g1}}{T_{g0}}=\left(1+\frac{\gamma-1}{2}M_0^2\right)\left(\frac{2\gamma}{\gamma-1}M_0^2-1\right)\left[M_0^2\frac{(\gamma+1)^2}{2(\gamma-1)}\right]^{-1} \tag{25}$$

$$M_1=\left(M_0^2+\frac{2}{\gamma-1}\right)\Big/\left(\frac{2\gamma}{\gamma-1}M_0^2-1\right) \tag{26}$$

$$u_1=M_1\sqrt{\gamma RT_{g1}} \tag{27}$$

$M_0$ and $M_1$ are the flow Mach numbers immediately ahead and behind the shock front.

## Final conditions

As mentioned, the extent of the relaxation zone in the case of a dusty gas is infinitely long for the equilibrium values are approached asymptotically. However, as shown by Gottlieb and Coskunses,[5] the suspension equilibrium properties at infinity can be calculated very simply by using Equations 23 to 27 and replacing $\gamma$ by $\bar{\gamma}$ and $R$ by $\bar{R}$. In this approach the multiphase suspension is assumed to be a single-phase gas having new values for $\gamma$ and $R$. Based on Gottlieb and Coskunses,[5] the relations for $\bar{\gamma}$ and $\bar{R}$ are

$$\bar{\gamma}=\frac{\Sigma\eta_iC_i+(1-\Sigma\eta_i)C_p}{\Sigma\eta_iC_i+(1-\Sigma\eta_i)C_v} \tag{28}$$

$$\bar{R}=(1-\Sigma\eta_i)R \tag{29}$$

where

$$\eta_i=\frac{\rho_{pi}}{\Sigma\rho_{pi}+\rho_g} \tag{30}$$

Note that in many papers the loading ratio is defined as $\eta_i^*=\rho_{pi}/\rho_g$. Thus, the two different definitions can be related by

$$\eta_i=\frac{\eta_i^*}{\Sigma\eta_i^*+1} \tag{31}$$

(It is clear from these relations that if the total loading ratio $\Sigma\eta_i$ and heat capacity $C_i$ are constant, then $\bar{\gamma}$ and $\bar{R}$ are constant and hence the equilibrium properties at the end of the relaxation zone are identical.) These new values (i.e., $\bar{\gamma}$ and $\bar{R}$) yield a new speed of sound $\bar{a}$, which satisfies

$$\bar{a}_0<a_0=(\gamma RT_{g0})^{1/2}$$

Thus the flow Mach number ahead of the shock wave becomes $\bar{M}_0>M_0$. By replacing $\gamma$, $R$, and $M_0$ in Equations 23 to 27 with $\bar{\gamma}$, $\bar{R}$, and $\bar{M}_0$, one can calculate the equilibrium properties of the suspension at infinity.

The knowledge of the suspension properties at infinity (i.e., the equilibrium final conditions) can serve as an excellent means of checking the reliability of the numerical results since they should be approached asymptotically.

Since the equilibrium conditions at infinity are known a priori, the integration was terminated when the suspension properties came as close as 2% of their corresponding equilibrium values. The distance where the velocities reached this condition is called the kinematic relaxation length $l_v$, and the distance where the temperatures reached this condition is called the thermal relaxation length $l_T$. These two relaxation lengths are in general different.

## Physical properties of the various phases

The gaseous phase was chosen to be nitrogen. Yun, Weissman, and Mason[13] have calculated the transport properties of nitrogen and presented their results in a tabular form for both $\mu_g$ and $k_g$. A least square polynomial fit to their results yields the following expressions for $k_g$ and $\mu_g$:

$$k_g[\mathrm{W/(mK)}]=1.386\times10^{-2}+(5.311\times10^{-5})T_g-(9.822\times10^{-10})T_g^2$$

and

$$\mu_g[\mathrm{kg/(m\,s)}]=0.7226\times10^{-5}+(2.768\times10^{-8})T_g-(0.5933\times10^{-12})T_g^2$$

The expression for the specific heat capacity at constant pressure, $C_p$, was adopted from Sontag and Van Wylen[14]

$$C_p[\mathrm{m^2/(s^2\,K)}]=1.3686\times10^3-(2.786\times10^5)T_g^{-1}+(5.1741\times10^7)T_g^{-2}$$

In the above expressions $T_g$ is in Kelvins.

Five solid phases were chosen in order to numerically simulate the effect of nonuniformities of the solid particles on the flow field. Thus, in Equations 15 and 16, $n=5$ and each of Equations 9 to 21 represents five equations with $i=1, 2, \ldots, 5$.

Each solid phase is identified by three parameters. The diameter of its particles $D_i$, the heat capacity of it particles $C_i$, and their material density $\sigma_i$.

Nine different cases (for $M_0=1.5$) were investigated. They are shown in Tables 1 to 3. In Table 1 all the five solid phases have the same material density $\sigma_1=\sigma_2=\cdots=\sigma_5=\sigma$ and heat capacity $C_1=C_2=\cdots=C_5=C$ but different particle diameters $D_1=5\,\mu$m, $D_2=7.5\,\mu$m, $D_3=10\,\mu$m, $D_4=25\,\mu$m, and $D_5=50\,\mu$m. The seven cases shown in Table 1 differ in the loading ratios of the various solid phases.

The partial loading ratios $\eta_i$ are chosen in such a way that the total loading ratios for each case (i.e., $\eta_{\text{total}}=\sum_1^5\eta_i$) always equals 0.2.

Thus, for all seven cases, the suspension properties should reach the same equilibrium values at the end of the relaxation zone.

In the case shown in Table 2 also for $M_0=1.5$, the five solid phases have identical particle diameters $D=50\,\mu$m, and material densities $\sigma=1500\,\mathrm{kg/m^3}$, but different heat capacities: $C_1=100$,

**Table 1** The loading ratios $\eta$ of the various size particles for $\sigma = 1500\,\text{kg/m}^3$ and $C = 1000\,\text{J/(kg K)}$

| | $D_i \times 10^6$ [m] | | | | | Case number |
|---|---|---|---|---|---|---|
| | 5 | 7.5 | 10 | 25 | 50 | $M_i$ |
| $i$ | 1 | 2 | 3 | 4 | 5 | 1.5 |
| | 0.04 | 0.04 | 0.04 | 0.04 | 0.04 | 1 |
| | 0.03 | 0.04 | 0.06 | 0.04 | 0.03 | 2 |
| | 0.06 | 0.05 | 0.04 | 0.03 | 0.02 | 3 |
| $\eta$ | 0.02 | 0.03 | 0.04 | 0.05 | 0.06 | 4 |
| | 0.099 | 0.06 | 0.03 | 0.01 | 0.001 | |
| | 0.001 | 0.01 | 0.03 | 0.06 | 0.099 | 6 |
| | — | — | 0.20 | — | — | 7 |

**Table 2** The specific heat capacities $C$ of the five various solid phases

| $C_i$ [J/(kg K)] | | | | | |
|---|---|---|---|---|---|
| 1 | 2 | 3 | 4 | 5 | Case number |
| 100 | 500 | 1000 | 5000 | 10,000 | 8 |

For all the solid phases $M_0 = 1.5$, $D = 50 \times 10^{-6}$ m, $\sigma = 1500\,\text{kg/m}^3$, $\eta = 0.04$.

**Table 3** The dust material densities $\sigma_i$ of the five various solid phases

| $\sigma_i$ [kg/m$^3$] | | | | | |
|---|---|---|---|---|---|
| 1 | 2 | 3 | 4 | 5 | Case number |
| 1000 | 1250 | 1500 | 1750 | 2000 | 9 |

For all the solid phases $M_0 = 1.5$, $D = 10 \times 10^{-6}$ m, $C = 1000\,\text{J/(kgm K)}$, $\eta = 0.04$.

$C_2 = 500$, $C_3 = 1000$, $C_4 = 5000$ and $C_5 = 10{,}000\,\text{J/(kg K)}$. The loading ratio of each solid phase is $\eta = 0.04$ and therefore the total loading ratio is again 0.2.

The last case is shown in Table 3. Here all the solid phases have identical particle diameters, $D = 10\,\mu$m, and heat capacities, $C = 1000\,\text{J/(kg K)}$, but different material densities: $\sigma_1 = 1000$, $\sigma_2 = 1250$, $\sigma_3 = 1500$, $\sigma_4 = 1750$, and $\sigma_5 = 2000\,\text{kg/m}^3$. The incident shock wave Mach number is again $M_0 = 1.5$, and the total loading ratio is 0.2 ($\eta_i = 0.04$ for each solid phase).

## Numerical results and discussions

### *Distribution of the diameter of the dust particles*

Figures 2 to 7 illustrate the flow field properties which are developed behind a normal shock wave with $M_0 = 1.5$ in cases 1 to 6, respectively (see Table 1). Each figure contains six velocity and six temperature profiles (one for the gaseous phase labeled with G and five for each of the five solid phases labeled 1 to 5 in accordance with Table 1) and one pressure profile. The dashed lines in the right sides of Figures 2 to 7 indicate the equilibrium values at infinity, which should be approached asymptotically. As mentioned earlier, these values are calculated a priori.

It is clear from Figures 2 to 7 that the larger the particle diameter is, the longer it takes for it to reach a dynamic

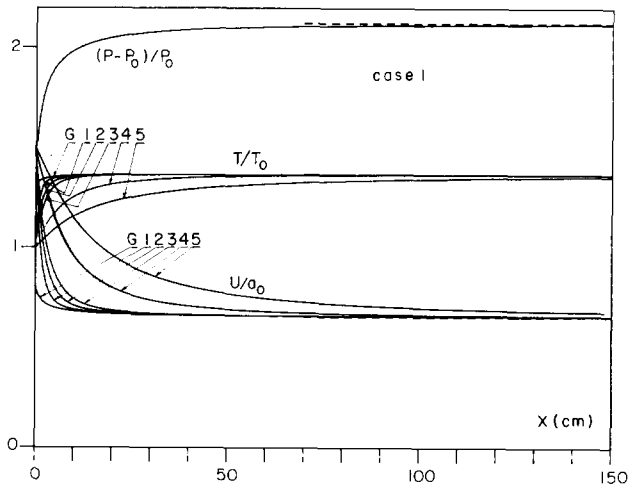


*Figure 2* Flow field for case 1 of Table 1

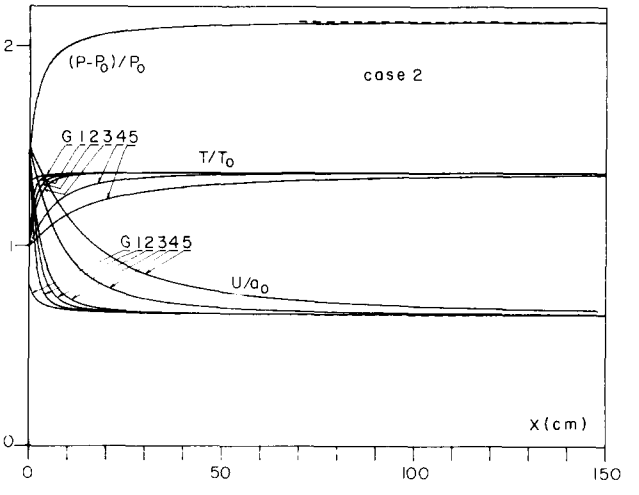


*Figure 3* Flow field for case 2 of Table 1

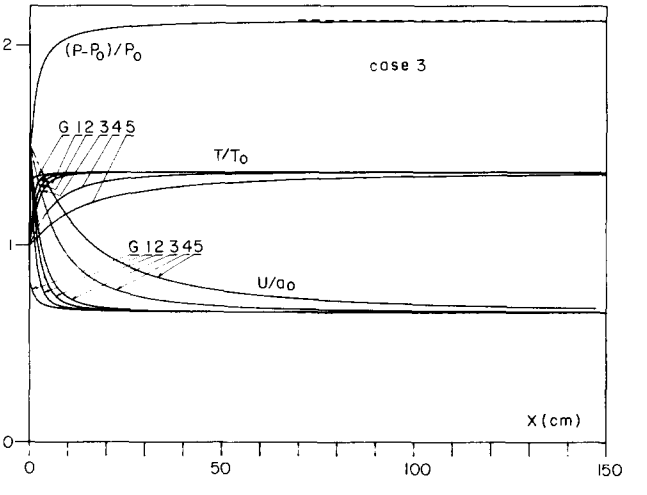


*Figure 4* Flow field for case 3 of Table 1

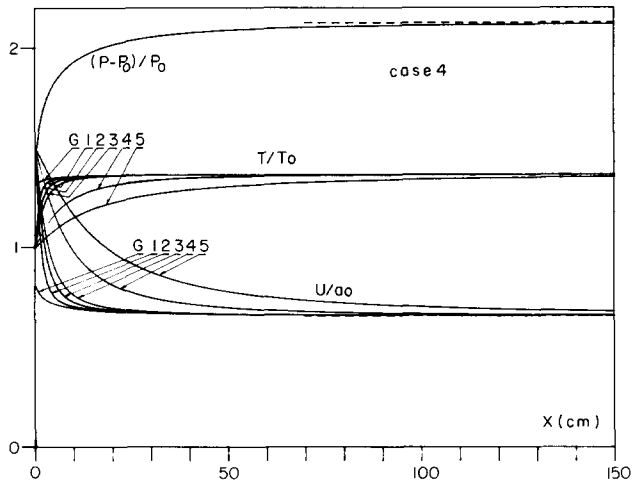


*Figure 5* Flow field for case 4 of Table 1

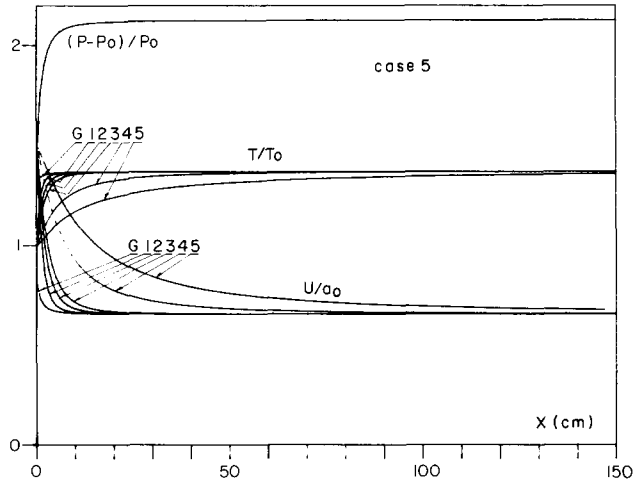


*Figure 6* Flow field for case 5 of Table 1

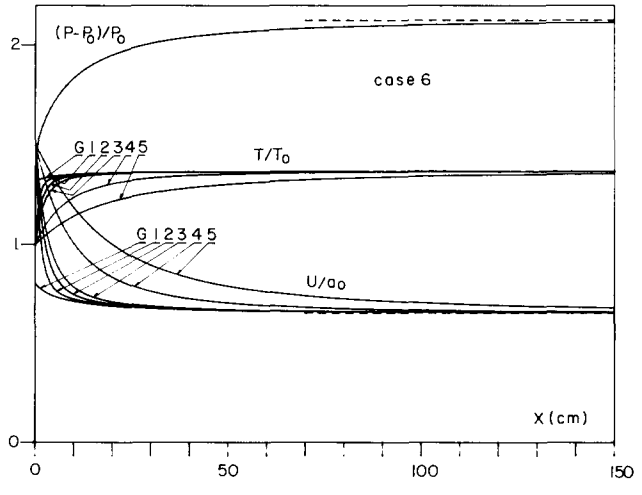


*Figure 7* Flow field for case 6 of Table 1

equilibrium. This is due to the fact that the inertia force depend on $D_1^3$, while the drag forces are roughly proportional to $D_1^2$. Thus the effectiveness of the drag forces in slowing down the solid particles decreases as the diameter of the solid particles increases. The solid phase with the larger particles is also the last to reach thermal equilibrium with the gaseous phase. This is not surprising since the larger the solid particle is, the slower will be its temperature rise. Thus the solid phase with the smallest particles ($D = 5\ \mu$m) reaches a thermal equilibrium with the gaseous phase within a few centimeters, while it takes tens of centimeters for the solid phase with the largest particles.

The velocity, temperature, and pressure profiles of the gaseous phase for cases 1 to 6 are shown in Figure 8. We clearly see that all six cases approach asymptotically identical equilibrium properties at infinity. This fact should not be surprising for the total loading ratio in all cases is $\eta = 0.2$, and the heat capacity of the solid particles is the same. Although the equilibrium properties are identical, the flow properties inside the relaxation zone do depend on the size distribution of the particles of each solid phase. The dependence is minimal for the gas temperature where the six profiles merge into almost one curve, and it is maximal for the suspension pressure. The suspension pressure increases very sharply when it consists mainly of small particles (case 5), and it increases very slowly when it consists mainly of large particles (case 6). Thus it can be concluded that increasing the mass fraction of the small solid particles in the suspension results in a faster rise in the suspension pressure. Similarly, the suspension with the largest amount of small particles results in the sharpest decrease in the gaseous phase velocity. The suspension with the largest amount of large particles experiences the slowest decrease in the gaseous phase velocity. The gaseous phase velocity falls from its value immediately behind the shock front even though it exchanges momentum with the solid phases which have much higher post-shock velocities. The reason for this peculiar behavior is that the dust presence causes a very large increase in the density of the gaseous phase. This in turn results in a large decrease in the gaseous phase velocity since the flow field is one-dimensional and $\rho_g u$ must remain constant.

The general shapes of the various property profiles, for the six cases of multisolid phases, are similar to those obtained when the suspension contains a single solid phase only, i.e., case 7 in Table 1, whose solution is seen in Figure 9. Since for this case $\eta = 0.2$ too, the equilibrium properties at infinity are identical to those shown in Figures 2 to 7.

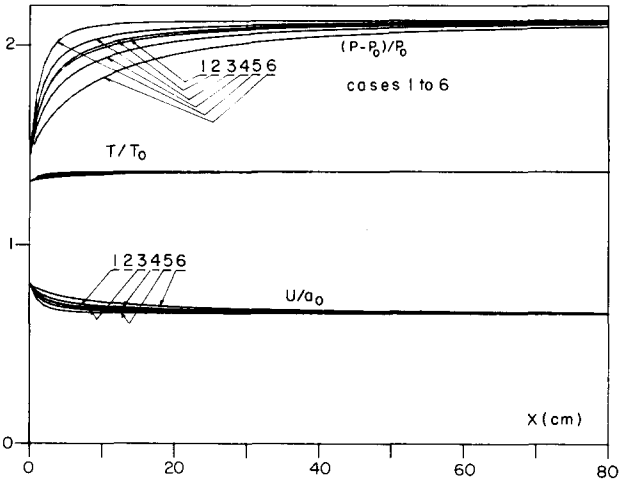


*Figure 8* Gas properties for cases 1 to 6

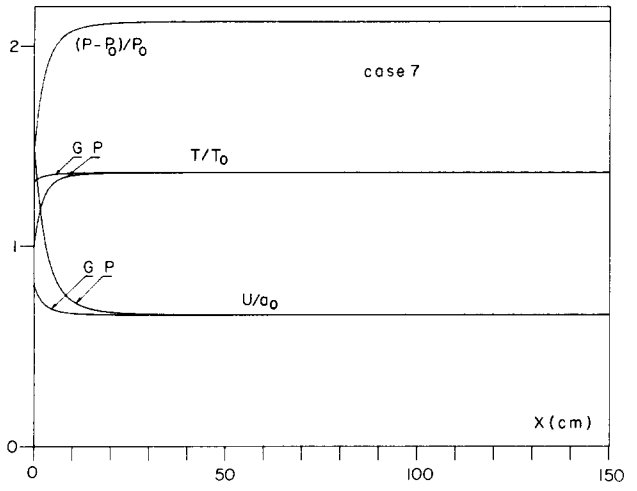


*Figure 9* Flow field for case 7 of Table 1

**Table 4** The thermal, $l_T$, and kinematic, $l_Y$, relaxation lengths for the nine cases in Tables 1, 2, and 3

| Initial condition in table | Case number | $l_T$ (m) | $l_Y$ (m) |
|---|---|---|---|
| | 1 | 1.91 | 3.83 |
| | 2 | 1.91 | 3.80 |
| | 3 | 1.90 | 3.75 |
| 1 | 4 | 1.92 | 3.90 |
| | 5 | 1.89 | 3.72 |
| | 6 | 1.92 | 4.05 |
| | 7 | 0.13 | 0.31 |
| 2 | 8 | 37.18 | 10.4 |
| 3 | 9 | 0.162 | 0.39 |

The thermal and kinematic relaxation lengths for cases 1 to 7 are given in Table 4. The earlier remark that the temperature of the gaseous phase is almost unaffected by the size distribution of the particles of the solid phases (see Figure 8, where all the temperature profiles merge into a single line at a very short distance behind the shock fronts) is further supported by the fact that the thermal relaxation lengths $l_T$ is almost the same for the six multiphase cases.

The difference between the kinematic relaxation lengths $l_Y$ is much larger. The two extreme cases, 5 and 6, differ by about 8.5%. Note that the difference in the thermal relaxation length between the two extreme cases is only about 1.5%.

However, the difference in both the thermal and kinematic relaxation lengths between the multisolid phases (cases 1 to 6) and the single solid phase (case 7) is enormous. Both $l_T$ and $l_Y$ are more than 90% smaller when the suspension contains a single solid phase with $D=10\,\mu$m. It is obvious that the enormous increase in both $l_T$ and $l_Y$ when the suspension contains a size distributed solid phase arises from the presence of the large particles, $D=50\,\mu$m, in the six cases. This is due to the fact that the large particles slow down and heat up very slowly in comparison with smaller particles. Thus it can be concluded that the extent of the relaxation zone is determined solely by the solid particle having the largest diameter.

### *Distribution of the heat capacity of the dust particles*

Case 8 (Table 2), in which the solid particles of the five phases have identical diameters $D=50\,\mu$m and material density $\sigma=1500\,\text{kg/m}^3$ but different heat capacities $C$ is shown in Figure 10 for $M_0=1.5$.

It is evident from Figure 10 that although the heat capacity $C$ of each of the solid phases is different, they all have the same velocity and pressure inside the relaxation zone. Thus, the heat capacity has no affect on the velocities of the solid particles and the gaseous phases and does not affect the suspension pressure. However, the five solid phases have different temperature profiles. The temperature of the solid particles with the highest value of $C$ experiences the slowest increase. For the smallest value of $C$ the temperature rise of the solid particles is extremely sharp. It overshoots the temperature of the gaseous phase before it drops down to the equilibrium value at infinity.

The thermal and kinematic relaxation lengths $l_T$ and $l_Y$, are also shown in Table 4 for this case (case 8). The large values for $l_T$ arise because it takes a long time for the solid phase with the largest heat capacity to reach equilibrium with the gaseous phase because their temperature rise is very slow. The large values for the kinematic relaxation length are due to the fact that the diameter of all the solid particles was chosen to be $D=50\,\mu$m for this case.

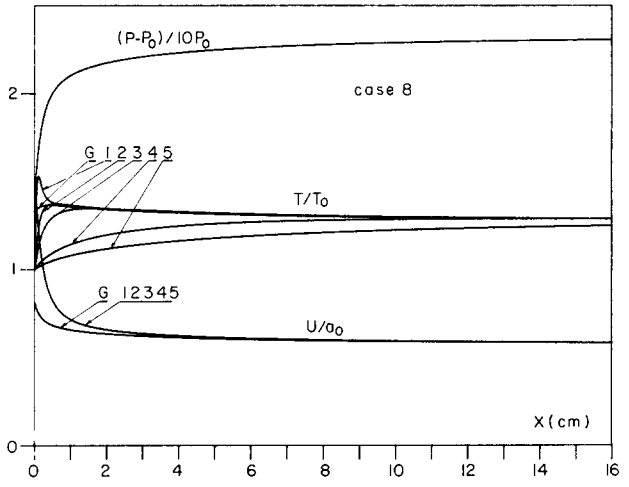


*Figure 10* Flow field for case 8 of Table 2

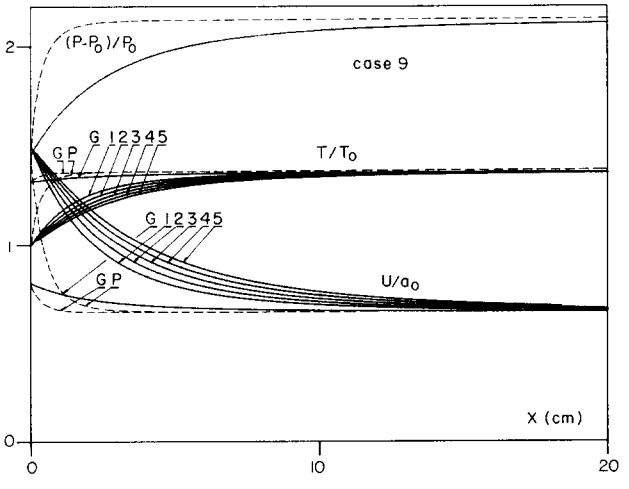


*Figure 11* Flow field for case 9 of Table 3

### *Distribution of the material density of the dust particles*

Case 9 (Table 3) in which the solid particles of the five phases have identical diameters $D=10\,\mu m$ and heat capacities $C=1000\,J/(kg\,K)$ but different material densities is shown in Figure 11 for $M_0=1.5$. Case 7 which has identical values of $D$ and $C$, as well as the total loading ratios of $\eta=0.2$, but a constant value of $\sigma=1500\,kg/m^3$, is added to Figure 11 in dashed lines.

The solid lines in Figure 11 indicate that the distribution in the solid particles density results in a decrease in the gas pressure, temperature, and velocity gradients behind the shock front. The equilibrium values, however, at infinity are identical for the two cases. In addition, it is evident from Figure 11 that the larger the material density of the dust particles is, the slower its decay becomes. This is so because its inertia depends linearly on the material density. Similarly, the larger the material density of the dust is, the slower its temperature rise becomes, because it has a higher heat capacity. The effect of the distribution in the material density of the dust particles on $l_T$ and $l_Y$ can be seen by comparing cases 7 and 9 in Table 4. For the $M_0=1.5$ case (7 and 9) both $l_T$ and $l_Y$ increase by about 25%.

## Conclusions

The flow field which is developed behind a steady normal shock wave in a dust-gas suspension has been solved numerically while accounting for distributions of nonuniformities in the physical properties of the solid phase. The model was based on a multiphase system which consists of one gaseous phase and five solid phases. The five solid phases differed from each other by one physical property only, which was either the diameter of the solid particles or their heat capacity or their material density.

For a fixed total loading ratio it was found that the gas temperature profile downstream of the shock wave is practically independent of the size distribution of the dust particles. This might also be a result of the relatively small loading ratio which was used in the calculation. Consequently, it should not necessarily hold for an arbitrary loading ratio. The suspension pressure profile, however, is very sensitive to the size distribution. The suspension pressure rises very sharply when the suspension contains mostly small particles. Similarly, the suspension with the largest amount of small particles results in the sharpest decrease in the velocity of the gaseous phase.

A distribution in the heat capacity of the solid particles resulted in a minor effect on the velocity of the solid particles and practically no effect on the suspension pressure. The effect on the temperature of the solid particles was much more pronounced. As expected, the particles with the smaller heat capacity were heated faster and their temperature reached that of the gaseous phase earlier than those having larger heat capacities.

A distribution in the material density of the solid particles resulted in different velocity and temperature profiles for each of the five solid phases and a slower rise in the suspension pressure.

## Acknowledgment

The financial support received from the U.S. Air Force under Grant AFOSR-86-0349 is acknowledged with thanks.

## References

1 Soo, S. L. *Fluid Dynamics of Multiphase Systems*, Blaisdell, Waltham, Mass., 1967
2 Marble, F. E. *Ann. Rev. Fluid Mech.* 1970, **2**, 397
3 Rudinger, G. *App. Mech. Rev.* 1973, **26**, 273
4 Morgenthaler, J. H. In *Progress in Astronautics and Rocketry*, eds. S. S. Penner and F. A. Williams, vol. 6. Academic Press, New York, 1962, p. 145
5 Gottlieb, J. J. and Coskunses, C. E. *UTIAS Rep. 295*, 1985
6 Carrier, G. F. *J. Fluid Mech.* 1958, **4**, 376
7 Kriebel, A. R. *J. Basic Eng., Trans. ASME* 1964, **D86**, 655
8 Rudinger, G. *Phys. Fluids* 1964, **7**, 658
9 Igra, O. and Ben-Dor, G. *Israel J. Tech.* 1980, **18**, 159
10 Ben-Dor, G. and Igra, O. *J. Plasma Phys.* 1982, **27**, 377
11 Igra, O. and Ben-Dor, G. *J. Plasma Phys.* 1984, **31**, 115
12 Elperin, I., Ben-Dor, G., and Igra, O. *ASME J. Fluid Eng.* 1986, **108**, 354
13 Yun, K. S., Weissmann, S., and Mason, E. A. *Phys. Fluids* 1962, **5**, 672
14 Sontag, R. E. and Van Wyler, G. J. *Introduction to Thermodynamics*, John Wiley and Sons, New York, 1971